

Chemical Treatment of Sn-Containing Transparent Conducting Oxides for the Enhanced Adhesion and Thermal Stability of Electroplated Metals


Ibbi Y. Ahmet,* Fatwa F. Abdi, and Roel van de Krol

A surface treatment process, named ReTreat, is presented, and is shown to enhance the adhesion of electroplated metals on Sn-containing transparent conducting oxides (TCOs). The ReTreat process uses Zn powders, FeSO₄ and glycine-buffered aqueous solutions (pH 3 to 5) in order to regulate a controlled and uniform conversion of SnO₂ surfaces to SnO, Sn metal, and Fe_xSn_y alloys. These surface metallic and intermetallic layers selectively enrich the electroplating of metallic films (including Ni, Au, and Ag). Subsequently, the process has been used to fabricate thermally stable metal films on rigid FTO-coated glass and flexible ITO-coated PET substrates. Standardized testing confirms that the metallic coatings exhibit sufficient adhesion to the underlying TCO with high thermal stability and tolerance to flexural strain. A reaction mechanism for the heterogenous surface treatment is deduced from X-ray diffraction, X-ray photoelectron spectroscopy, and in situ transmittance measurements. These investigations show how the process parameters (e.g., Zn powders, FeSO₄ concentration, pH, and TCO type) impact the reaction rate, morphology, and composition of the treated TCO surface. This report provides detailed insights necessary for the future implementation of this innovative surface treatment, which has the prospect to be a customary process for electroplating onto Sn-containing TCOs.

1. Introduction

Transparent conducting oxide (TCO) thin films are one of the most prevalent functional materials used in optoelectronic devices, due to their combined properties of high transparency for visible light, good electrical conductivity, and high thermal stability.^[1,2] The dominant commercial technologies using TCOs are flat panel displays (FPDs) and touch screens,^[3] photovoltaics, and architectural low emission glass coatings (Low-E glass).

I. Y. Ahmet, F. F. Abdi, R. van de Krol
Institute for Solar Fuels
Helmholtz-Zentrum Berlin für Materialien und Energie GmbH
Hahn-Meitner-Platz 1, 14109 Berlin, Germany
E-mail: ibrahim.ahmet@helmholtz-berlin.de

 The ORCID identification number(s) for the author(s) of this article can be found under <https://doi.org/10.1002/admi.202201617>.

© 2022 The Authors. Advanced Materials Interfaces published by Wiley-VCH GmbH. This is an open access article under the terms of the Creative Commons Attribution License, which permits use, distribution and reproduction in any medium, provided the original work is properly cited.

DOI: 10.1002/admi.202201617

These applications have driven the demand for increasingly large areas, requiring scalable and robust manufacturing processes. Furthermore, the number of new optoelectronic technologies into which TCOs are integrated is continuously growing.^[4] The most common n-type TCOs are composed of doped metal oxides, such as zinc oxide (ZnO), tin oxide (SnO₂), or indium oxide (In₂O₃). For example, fluorine-doped tin oxide (FTO), deposited by pyrolytic chemical deposition processes, is an archetypal substrate/back-contact for metal oxide photoelectrodes and has been widely used for solar driven photoelectrochemical (PEC) water splitting.^[2,5] Depending on the crystallinity, film thickness, and concentration of the fluoride dopant, the sheet resistance of FTO typically ranges from 7 to 15 Ω sq⁻¹, while exhibiting sufficient chemical and thermal stabilities (up to 700 °C on quartz substrates).^[6] Indium tin oxide (ITO) is another common TCO used in high efficiency photovoltaic (PV) technologies, due to its higher optical transmittance, reasonable mechanical stability on flex-

ible substrates,^[7] reasonable conductivities (3–60 Ω sq⁻¹),^[8] and high thermal stability (up to 800 °C on quartz substrates).^[8,9] However, ITO is less chemically stable than FTO in aqueous solutions, which limits its use in (photo)electrochemical applications. Moreover, due to the scarcity and the higher price of indium, the use of ITO-based TCOs for large-scale applications can be economically challenging.^[10]

Despite the relatively good conductivities of TCOs, their use in most optoelectronic devices still introduces noticeable ohmic losses, especially when the device area is scaled up beyond 1 cm².^[11] In devices such as touch screens, printed circuit boards (PCB), photovoltaic panels or photoelectrodes, these ohmic losses can be minimized by depositing metallic contacts, interconnects, or busbars that typically consist of stable metals or alloys (e.g., Cu, Ag, Ni, Al, Sn, and Au) with higher specific conductivities (≈10⁷ S m⁻¹).^[3,12,13] Here, the interconnects' architecture (i.e., arrangement, distribution, width, thickness), which is usually a trade-off between optical transmittance, available space, ohmic resistance and electronic interference,^[14–16] can be optimized to maximize device performance.

Metallic interconnects have been deposited onto TCOs using various methods, including spray deposition,^[17] thermal

evaporation, sputtering,^[18] physical and chemical vapor deposition,^[15,19] nanoparticle inkjet printing, screen printing,^[20] and solution-based electro- or electroless deposition.^[12,19,21–23] One of the main challenges for the development of suitable deposition processes is the delamination of the metallic coating from the underlying TCO film. A vast number of methods have been developed to enhance adhesion and prevent delamination. These include routes such as inverted film processing,^[22,23] sealing and lamination,^[24] trench etching and increasing the surface roughness,^[18,22,25] surface (plasma-)cleaning,^[26] interfacial seed layers or organic adhesives, and chemical surface treatment or surface “activation.”^[25,27] The number of patents and research publications aimed at addressing this adhesion issue is extensive. Therefore, below we will only discuss several selected publications focusing on surface treatments that improve the adhesion of metallic thin films electrodeposited onto Sn-containing TCOs, such as ITO and FTO.^[28]

Early work in the 1990s by Laverty and Molloy et al. presented an electrochemically reductive treatment method for FTO thin films prior to electroplating with Cu.^[29] In this report, FTO-coated glass substrates were placed inside a pH ≈ 1 acidic electrolyte containing 0.01 M Na₂SO₄ and 0.1 M H₂SO₄, and subjected to a galvanostatic cathodic current density of ≈25 mA cm⁻² for a short duration (5 to 10 s). The authors reported that during the reductive treatment, a black layer formed consisting of a mixture of Sn and SnO, which then instantaneously dissolved in the acidic solutions. After treatment, the adhesion and quality of the Cu plating were significantly improved. The resulting metallic Cu films, produced at lower electroplating current densities, were stable to thermal stress. They also passed the “Scotch tape” test and exhibited adhesion strengths greater than 100 kg cm⁻² (determined from the z-axis stud pull method).^[3,29] The enhanced adhesion was attributed to a combination of factors, including: 1) an increased mechanical interlock between the rough etched FTO surface and electroplated Cu, 2) the greater cohesive bonding between the residual metallic Sn and Cu, and/or 3) the formation of a lower-valence tin oxide (SnO or SnO_{2-x}) surface layer, which leads to the removal of hydroxyl groups and generates reactive peroxide bonds, or Sn²⁺ cations. The authors, however, mentioned two main limitations of this electrochemical approach. First, they observed nonuniform etching and reduction of the FTO across larger area samples. Furthermore, at high applied current densities, they observed over-etching close to the electrical contacts, which removed most of the FTO film.

Similarly, a patent published by Zaban et al. in 2012 describes an electrolysis pre-treatment process that reduces the upper layer of TCOs, including ITO and FTO, and can significantly improve the adhesion and stability of electroplated NiCo alloys.^[25] Using this pre-treatment process, they fabricated metallic interconnects, buried between the TCO and a photo-absorber layer, which were able to withstand sintering temperatures as high as 550 °C. The explanations provided for the enhanced adhesion are similar to those provided by Laverty and Molloy et al. Furthermore, a subsequent patent by Zaban et al. published in 2015 describes an alternative chemical sensitizing method which activates/reduces the TCO surface using a solution containing reductive cations, such as tin (II) (e.g., SnCl₂) or titanium (III) salts (e.g., TiCl₃), with a preference towards

SnCl₂.^[27] This surface treatment leads to the reduction of SnO₂ to SnO and Sn, which is proposed to increase the cohesion caused by Van der Waals forces and adhesive bond strength at the TCO/metal interface after electroplating.

In relation to the surface treatment method presented in this manuscript, we must briefly discuss the Zn-assisted acid etching technique, which is widely used for selective etching of Sn-containing TCO layers at the laboratory and industrial scale.^[30,31] In summary, exposed regions of the TCO are coated with Zn powders, and then immersed in concentrated acid solutions, such as HCl. The SnO₂ is initially reduced by the Zn to metallic Sn, and the Zn powders simultaneously react with the acid solution to generate H₂ gas as a by-product. The metallic Sn then reacts with the concentrated HCl following an oxidative displacement reaction, resulting in the formation of SnCl₂ and the selective etching of the Sn-containing TCO layer often with high precision and minimal undercut. A number of publications and patents published as early as 1973 have described similar etching methods for processing Sn-containing TCOs for various optoelectronic devices.^[28]

The patent by McLean and Feldman published in 1999 describes a modification of the Zn-based TCO etching technique.^[32] Ferric (FeCl₃) or ferrous ions (FeCl₂) are added to the concentrated HCl etching solution, which enables greater control and uniformity of the TCO etching depth by slowing down the etching rate. In this case, Zn powders reduce Fe³⁺ ions to Fe²⁺. The Fe²⁺ ions are proposed to function as the intermediate reducing agent to convert SnO₂ to metallic Sn, which is then subsequently etched within the strong acid solution. Interestingly, an embodiment of the patent describes a process where the direct addition of a sufficiently high concentration of ferrous (Fe²⁺) ions (>0.01 M) can completely inhibit etching of the TCO, but results in the formation of a shiny “metallic” layer at the surface.^[32] To our knowledge, no subsequent characterization of this “metallic” TCO surface was reported, nor have there been follow-up publications providing a detailed analysis of this heterogeneous galvanic displacement reaction and its applications.

In the current study, we have investigated this process in more detail and developed a surface treatment process called ReTreat, which can be applied to enhance the adhesion of electrodeposited metals onto TCOs. Although we briefly described the ReTreat process in a previously published study and patent,^[16,33] here we provide a comprehensive understanding of the heterogeneous reaction between the ReTreat solution and Sn-containing TCOs that will allow others to fully exploit this process. The ReTreat process utilises aqueous glycine buffered solutions (pH 3 to 5) containing FeSO₄ in combination with metallic Zn powders (reducing agent). We present two optimized methodologies for pre-treating the surfaces of FTO on glass and ITO on polyethylene terephthalate (PET), and we show how this simple chemical pre-treatment can be implemented prior to electroplating metallic coatings and interconnects with various patterns at large scales on both rigid FTO-coated glass and flexible ITO-coated PET substrates. To further verify the improved quality of the metal coatings on the surface-treated TCOs, we have subjected the samples to various industrially standardized adhesion and thermal stress tests, including infrared (IR) reflow testing in N₂ and O₂ atmospheres, highly accelerated stress testing (HAST), as well as several standardized

adhesion tests described by the International Organization for Standardization (ISO). Furthermore, electroplated Ni and Au films on chemically treated FTO are shown to be able to withstand high temperatures (up to 450 °C) without delaminating nor loss in conductivity, making it possible to use these metallic coatings in subsequent high temperature fabrication steps. In addition, X-ray diffraction analysis (XRD) and X-ray photoelectron spectroscopy (XPS) analysis were used to determine the surface composition of the TCOs after chemical treatment. Furthermore, we describe a simple in situ transmittance analysis method to monitor the time-dependent changes in the TCO optical properties during the surface treatment. From this analysis, we have formulated a kinetic model and heuristic description of the heterogeneous reaction mechanism at the surface of Sn-containing TCOs during ReTreat.

2. Results and Discussion

2.1. Optimized Surface Treatment of Sn-Containing TCOs Prior Electrodeposition (ReTreat)

Figure 1 presents the two surface treatment methods optimized for treating either commercial FTO films on rigid glass substrates (Method 1) or ITO films on flexible PET substrates (Method 2). These surface treatment methods have been used within our research group as an adhesion promoter and to enhance the thermal stability of electroplated coatings on both FTO and ITO substrates. For both methods, the ReTreat process utilizes mildly acidic 1.0 M glycine-buffered aqueous solutions (pH 3 to 5) containing FeSO_4 with a concentration ranging from 0.1 to 1.0 M. However, there are clear differences

Reductive Surface Treatment Process (*ReTreat*)

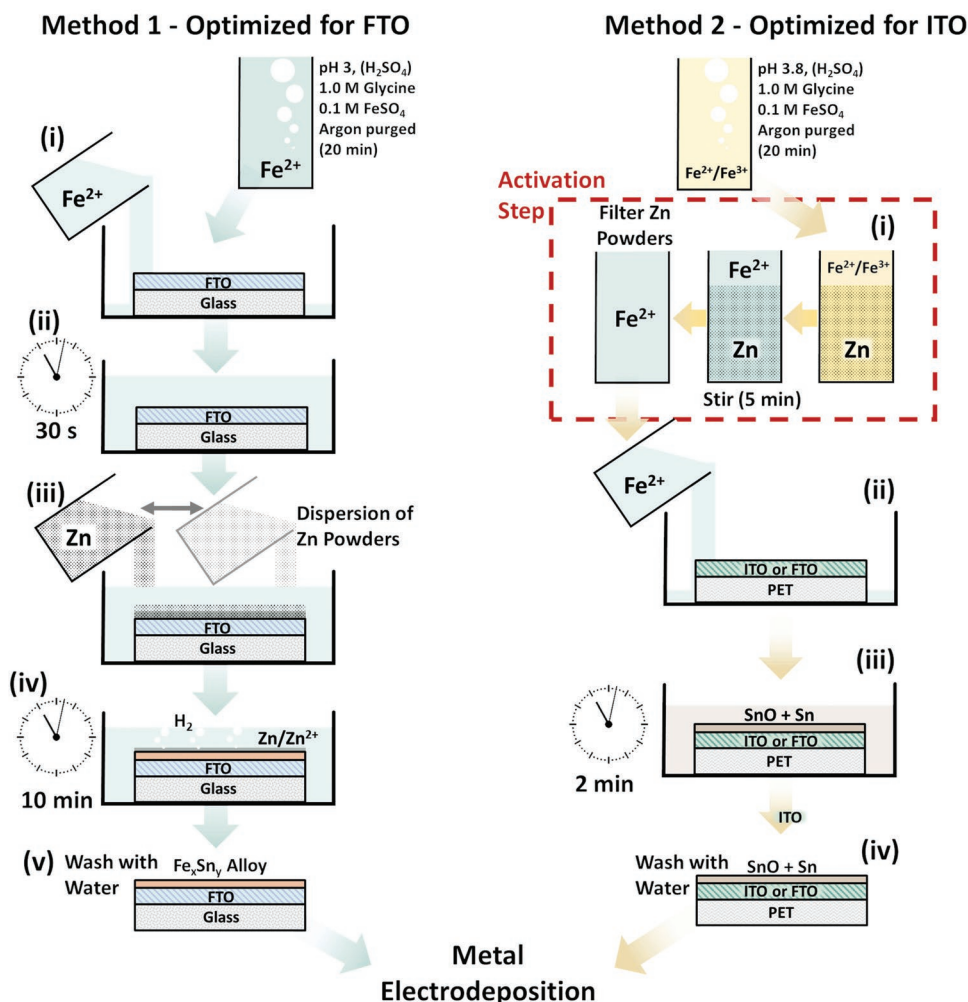


Figure 1. Summary of the two different ReTreat methods optimized for activating the surfaces of either FTO on glass (Method 1) or ITO on PET (Method 2) prior to electroplating. Method 1 generates a surface layer consisting of SnO, Sn, and Fe_xSn_y alloys. Method 2 reduces the SnO₂ to a mixture of SnO and Sn. The ReTreat process increases the selectivity of electroplating and enhances the adhesion and thermal stabilities of electroplated metals.

in the process steps between the two methods, which will be discussed in the following sections.

As mentioned, Method 1 was optimized for commercial FTO coated glass substrates (e.g., TEC 15 and TEC 7). This method typically utilizes treatment solutions with a pH \approx 3. It must be noted that using more acidic treatment solutions with a pH < 3 leads to over-etching of the TCO and generates a large amount of H₂ gas. On the other hand the surface treatment reaction rate decreases and eventually inhibited as the pH of the treatment solution increases above 3. A distinguishing feature of this method is that Zn powders are in direct contact with the FTO surface during treatment. In this case, Zn reduces both SnO₂ at the surface of the TCO as well as Fe²⁺ ions in solution, which results in the formation of an intermetallic surface that appears smooth and shiny (see Figure S1a and Video S1, Supporting Information).^[32] Figure S2 (Supporting Information) presents the XRD analysis of FTO substrates after surface treatment using ReTreat Method 1 with FeSO₄ concentrations ranging from 0.1 to 1.0 M. XRD peaks for the Fe_{0.74}Sn₅ and Fe₃Sn₂ intermetallic alloys were identified on the treated substrates, and the relative composition of the alloys is strongly affected by the concentration of FeSO₄ in the treatment solution. As the concentration of FeSO₄ in the treatment solution increases from 0.1 to 1.0 M, the diffraction peaks for the Fe_{0.74}Sn₅ phase become less intense and the peaks for a secondary intermetallic phase Fe₃Sn₂, with higher Fe content, become more pronounced. A similar trend was also reported elsewhere in the reductive synthesis of Fe_xSn_y intermetallic nanospheres.^[34]

Further analysis of the FTO samples before and after ReTreat Method 1 treatment by scanning electron microscopy (SEM), presented in Figure S3a–d (Supporting Information), shows that the morphology of the FTO surface becomes smoother, with smaller grains. The energy-dispersive X-ray spectroscopy (EDS) analysis, presented in Table 1 and Figure S4 (Supporting Information), shows that this surface treatment method deposits Fe onto the surface. A composition with a relative Sn:Fe ratio of 3:1 is obtained with a comparatively lower amount of O compared to the untreated FTO film. This observation agrees with the XRD analysis, and leads to the conclusion that Fe_xSn_y alloys are formed at the surface of FTO following Method 1. It is important to note that without FeSO₄ in the treatment solution, the FTO is etched after the dispersion of Zn powders,^[30] and a rough surface is formed, as shown by the SEM images in Figure S3e,f (Supporting Information).

Method 2 of the ReTreat process was optimized for commercial ITO-coated PET substrates (Video S2, Supporting

Information). This method utilizes solutions with a slightly higher pH of \approx 3.8. Increasing the pH was found to lower the surface reaction rate; a pH value of \approx 3.8 was found to be optimal to drive the surface reaction and at the same time prevents the complete etching of the polycrystalline ITO films, which occurs at pH < 3 lower (Figure S6, Supporting Information). Method 2 can also be used for treating FTO substrates, however longer treatment times (40 min with Method 2 versus 10 min with Method 1) are required due to the slower reaction rates. At pH 3.8 the Fe²⁺ cations in solution are unstable and are immediately oxidized by the residual oxygen in solution during the initial dissolution, even when the solutions are purged with N₂ or Ar. To prevent this, Method 2 requires an “activation” step. This step involves the addition of Zn powders to the FeSO₄ solutions followed by stirring to form a slurry. Resultantly the Fe³⁺ cations, which were formed by oxidation with residual oxygen are reduced back to Fe²⁺, as evidenced by a color change of the solution from pale orange to pale blue. After filtering the larger Zn particles, the ReTreat solution is then considered to be “activated.” The ITO-coated PET substrates can then be treated by immersing them in the activated solutions for a typical duration of 2 min. Further details on the experimental procedure are provided in Section S2 of the Supporting Information.

When using Method 2, the Zn powders are removed and not considered to be in direct contact with the ITO (or FTO) surface. After treatment, ITO (or FTO) substrates are washed with water and a pale brown coating becomes visible (Figure S1b, Supporting Information). In this case, the reactive Fe²⁺ cations mediate the reduction of SnO₂ to form an amorphous layer of Sn and SnO. The SEM images shown in Figure S3 (Supporting Information) (FTO) and Figure S7 (Supporting Information) (ITO) reveal that the surface treatment via Method 2 modifies the morphology of the TCO (FTO and ITO) and appears to partially etch the surface, causing an increase in the surface roughness. The etching of ITO becomes more pronounced and leads to partial amorphization when using a pH 3 solution (Figure S6, Supporting Information). Increasing the FeSO₄ concentration also leads to further amorphization of ITO, indicated by the broadening and relative decrease in the intensities of Bragg peaks assigned to ITO (Figure S8, Supporting Information). Using the same treatment on FTO substrates (Figure S9, Supporting Information) leads to changes in the relative intensities of diffraction peaks, such that there is a decrease in the relative intensity of the 110 (26.5°) and 101 (33.8°) peaks compared to the 200 (37.7°) peak. This may indicate that this surface treatment preferentially etches the 110 and 101 planes of the rutile

Table 1. Summary of the EDS surface quantification for FTO/glass and ITO/PET substrates before and after ReTreat surface treatment following Methods 1 or 2. The corresponding EDS spectra are presented within Figures S4 and S5 (Supporting Information).

Substrate	ReTreat Method	FeSO ₄ conc. [M]	pH	Composition from EDS [at. %]				
				In	Sn	O	Fe	Zn
FTO/glass (ref.)	–	–	–	–	27.76	72.24	–	–
FTO/glass	1 (Zn)	0.1	3	–	32.01	52.62	10.04	0.33
FTO/glass	2 (40 min)	0.1	3.8	–	31.87	68.13	–	–
ITO/PET (ref.)	–	–	–	42.91	4.91	52.68	–	–
ITO/PET	2 (2 min)	0.1	3.8	43.36	6.69	49.95	–	–

SnO₂ host structure of FTO. One must note, however, that the XRD analysis was conducted using a grazing incidence configuration (GIXRD), and therefore less accurate for characterizing changes in the orientation of polycrystalline films.

We do not observe the formation of Fe_xSn_y alloys at the surface when using Method 2 for both ITO and FTO films. From the EDS quantification of ITO and FTO surfaces after treatment with Method 2, we observe a decrease in the amount of oxygen, indicating a reduction of metal oxide (Table 1, and Figures S4 and S5, Supporting Information). This is further supported by the XPS analysis presented further on. From this we speculate that by removing the Zn powders prior to the surface treatment following Method 2, it is not possible to further reduce Fe²⁺ ions at the surface of the TCO to metallic Fe⁰, thus inhibiting the formation of Fe_xSn_y alloys at the surface of the respective Sn-containing TCOs.

2.2. Electroplating of Treated TCOs

The surface treatment methods discussed are applied as an adhesion promoter prior to electroplating onto the respective TCOs. The ReTreat process is found to be compatible with a range of masking materials, including photoresist and Kapton tape. In less critical applications, a permanent marker can also be used as a masking material (Figure S10 and Videos S1, S3, and S4, Supporting Information).

Different galvanostatic electroplating procedures were optimized for ReTreat treated FTO on glass and treated ITO on PET (Figure 2). These include electroplating procedures for nickel, gold, and silver coatings with a thickness of either ≈200 nm (Figure 2, and Figures S11 and S12, Supporting Information) or 1 μm (Figure S13, Supporting Information). Further details related to the electroplating methods can be found in the experimental section. Figure 2 and Figure S14 (Supporting Information) show photographs of a selection of samples that have been fabricated, which includes large area Ni, Au, and Ag mirrors, thermally stable Au and Ni interconnects on FTO-coated glass, and flexible Au films on ITO-coated PET substrates (Video S5, Supporting Information). The sheet resistances of all the metallic films were typically below 1 Ω sq⁻¹. By visual inspection, the metallic coatings show excellent homogeneity and good reflectivity. By using Kapton tape as a masking material, it is possible to apply the chemical treatment process and then electrodeposit metallic features with a line width of <50 μm, as shown in Figure S15 (Supporting Information). It is expected that smaller features can be achieved with more advanced masking and lithography techniques.

2.3. Enhanced Adhesion and Thermal Stability of Electroplated Layers

As shown in the previous section, the ReTreat process is found to generate metallic and intermetallic layers at the surface of the FTO and ITO. These metallic and intermetallic interfaces are shown to selectively enrich the deposition and adhesion of electrodeposited metallic films (Au, Ni, or Ag), whilst simultaneously enhancing the film quality and thermal stability (up to

450 °C). The treatment was also found to enhance the selectivity for subsequent electrodeposition steps; when both untreated and treated regions were exposed to the electrodeposition bath, the electroplated metal film would preferentially deposit on the regions that were treated. It is therefore expected that reduced metallic and intermetallic surfaces formed after treatment have a higher reduction potential and lower the activation energy required for initiating the electroplating.

We will first compare the properties of the electroplated metal films on FTO-coated glass substrates, before and after treatment with Method 1. The SEM micrographs in Figure S11 (Supporting Information) present a 200 nm thick Au film electroplated on an untreated and treated region of FTO. The films grown on the treated surfaces have a much smoother morphology with a smaller grain size compared to the Au films on the untreated region. Furthermore, Au films grown on untreated FTO region were found to delaminate while being exposed to the electron beam during SEM analysis (Figure S11d, Supporting Information); no such delamination was observed for the Au films deposited on the treated regions. For Ni and Au coatings on FTO substrates, initial adhesion tests were performed using Kapton tape (Figure 3 and Figures S16 and S17, and Video S6, Supporting Information). The adhesion is found to be significantly better for the metal films deposited on treated FTO. The metal coatings electrodeposited onto untreated FTO could easily be removed with tape or by scratching and wiping. Metal films grown on regions of the FTO treated with ReTreat remained attached to the FTO. Neither flaking nor delamination was observed even after the films are scratched. Ni films on untreated FTO also would delaminate during storage over 24 h, as shown in Figure S18 (Supporting Information), while the equivalent films on treated FTO remained stable and adhered to the surface (even after storage in air for over 1 year).

Attempts to electrodeposit Ni and Au films onto untreated ITO-coated PET substrates were unsuccessful. During electroplating, the metal films would delaminate or lead to patches of adhered metal layers that could be wiped off during cleaning. It was therefore challenging to produce metal films on untreated ITO substrates, even when using different galvanostatic current densities. Interestingly, after surface treatment of the ITO using ReTreat method 2 (Figure 1), both Ni and Au films could be deposited onto ITO-coated PET. The Au films displayed improved adhesion and displayed high tolerance to multiple bending cycles (>200 times) and folding (bend radius ≈1 mm) without visible delamination (Figure 2 and Figure S19, and Video S6, Supporting Information). In contrast, the Ni films on ITO-coated PET would form cracks when placed under both tensile and compressive stress, subsequently causing the layers to delaminate. The reason for the differences between the Ni and Au adhesion on treated ITO substrates was attributed to the different ductility of the metals. At room temperature, the ductility index of Au is 0.93, compared to 0.71 for Ni. The latter value indicates that Ni is close to its ductile-to-brittle transition point, and is therefore less tolerant to deformation and strain.^[35]

Standardized cross-hatching and tape adhesion tests were also conducted on the Au films electroplated on treated FTO-coated glass and ITO-coated PET substrates. As described in Table S1 (Supporting Information) and presented in Figures S20

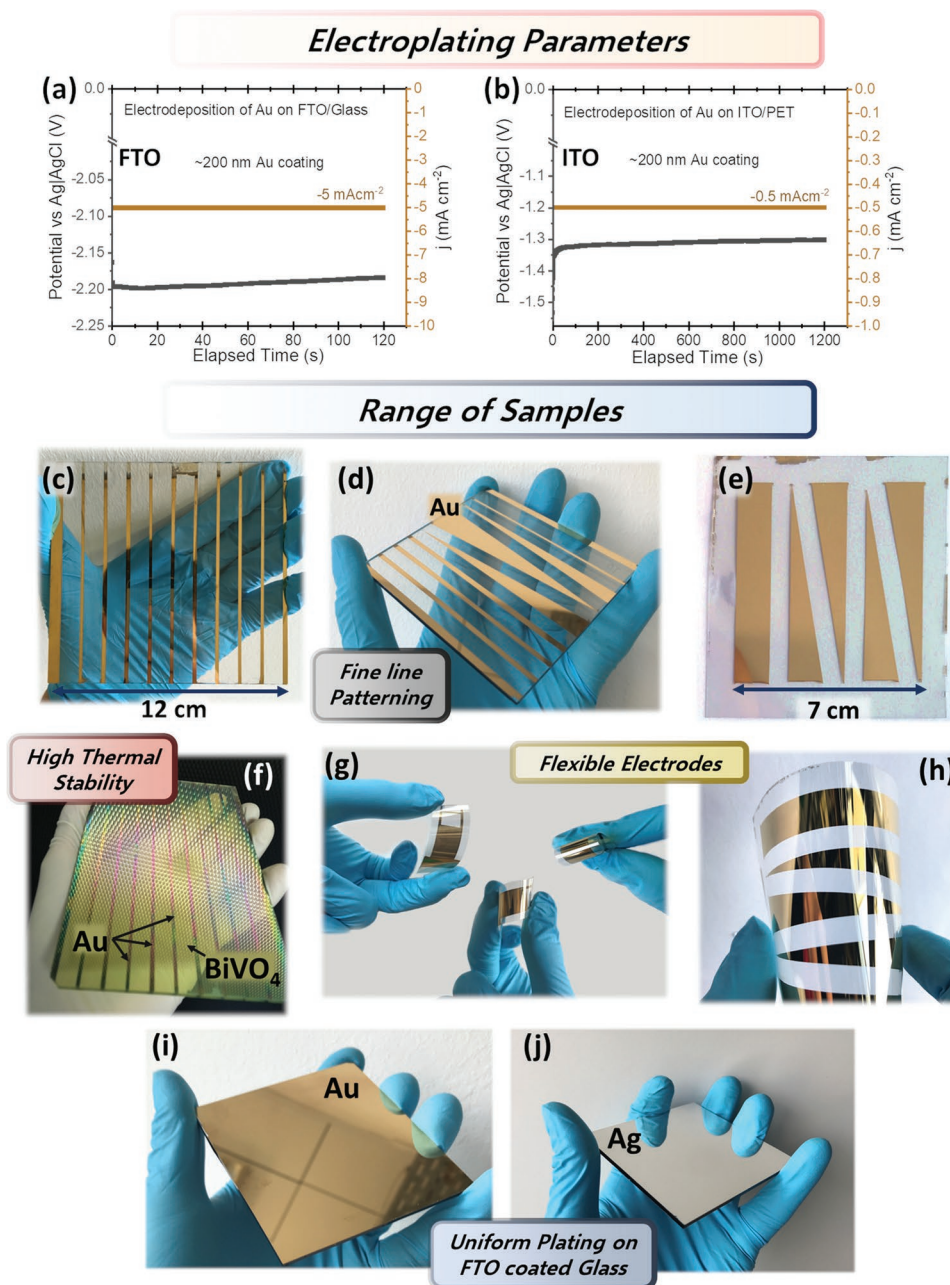


Figure 2. The galvanostatic deposition parameters for electroplating ≈ 200 nm thick Au films on pre-treated a) FTO on glass or b) ITO on PET, with a deposition area of 90 cm^2 and 20 cm^2 , respectively. Photographic images of c) Au interconnects electrodeposited onto FTO coated glass, Au interconnects with a variety of line widths, on d) pre-treated FTO coated glass (Method 1) and e) pre-treated ITO coated PET (Method 2), f) large area BiVO₄ photoanode with Au interconnects. g,h) Flexible electroplated Au films on pre-treated ITO coated PET substrates (Method 2). Reflective and uniform i) Au and j) Ag films electrodeposited on pre-treated FTO coated glass substrates with a $10 \times 10 \text{ cm}^2$ area (Method 1).

and S21 (Supporting Information), all samples achieved the highest adhesion classification, i.e., ISO 0 (ASTM 5B), with no material removed.

The Ni and Au coatings on treated FTO were also subject to thermal testing, which consisted of standardized highly accelerated stress testing (HAST) in air with 85% relative humidity at $130 \text{ }^\circ\text{C}$ for 95 h (type U IEC conditions), and multiple lead-free infra-red reflow (IR Reflow) cycles up to $\approx 260 \text{ }^\circ\text{C}$ in N₂ (6 cycles) and O₂ (2 cycles), following the temperature profile in Figure S22 (Supporting Information). Further details are given in the

experimental section. Following HAST and IR Reflow tests, both the Ni and Au coatings on treated FTO yielded excellent stability and adhesion (Figure S23, Supporting Information). In addition, the Ni and Au coatings on treated FTO proved to withstand thermal annealing on a hot plate up to $450 \text{ }^\circ\text{C}$ in air for 4 h (Figure S24, Supporting Information).

In comparison, the Au films electroplated on treated ITO-coated PET substrates also exhibited no signs of delamination after HAST or IR Reflow test conditions. However, the elevated temperatures during testing surpassed the glass transition

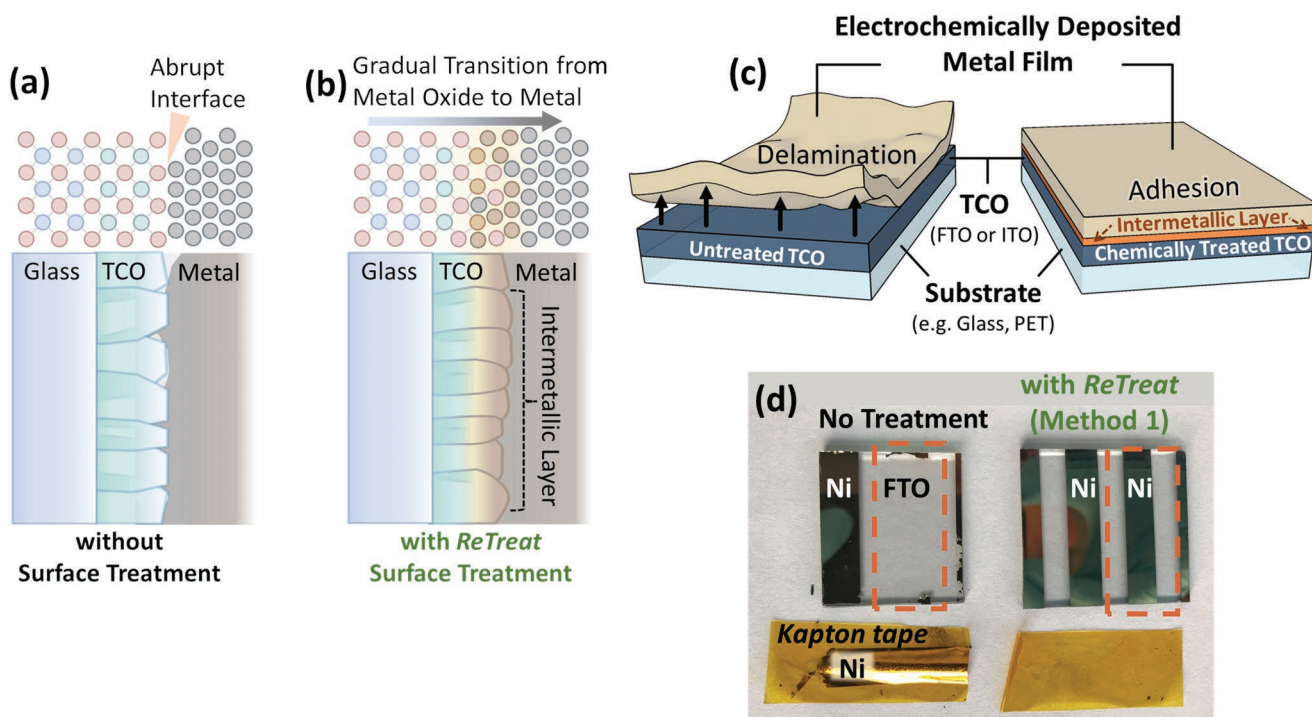


Figure 3. Illustration of the interface between the Sn-containing TCO and the electroplated metal a) without surface treatment and b) with ReTreat surface treatment, which forms an intermetallic layer gradually transitioning from metal oxide to metal. c) Illustration of how surface treatment and the intermetallic layer enhances the adhesion of electroplated metals. d) Kapton tape testing shows enhanced adhesion for the electrodeposited Ni layers on FTO-coated glass TCOs after ReTreat surface treatment.

temperature of PET ($T_g \approx 80^\circ\text{C}$) and resulted in the embrittlement of the substrates, causing them to fracture during bending (Figure S25 and Video S7, Supporting Information).

The poor adhesion of electroplated metal films on untreated TCOs is attributed to the abrupt metal oxide/metal interface formed after electroplating. The cohesive interaction between these interfaces is mostly mechanical in nature and subsequently much weaker (Figure 3). Whereas the improved adhesion after surface treatment is attributed to the reduction of SnO_2 to an intermetallic layer, and this leads to a gradual transition from metal oxide to metal at the TCO surfaces which enables stronger adhesive interactions between TCO/intermetallic/metal interfaces (Figure 3).

2.4. Chemical Nature of the TCO Surfaces after Surface Treatment with Different ReTreat Methods

The following sections will present further materials characterization comparing treated FTO and ITO surfaces. Furthermore, we discuss how the pH and FeSO_4 concentration in the ReTreat solution impacts the heterogeneous reaction kinetics and the resultant products formed at the surface.

X-ray photoemission spectroscopy (XPS) analysis of the FTO and ITO substrates before and after ReTreat, either using Method 1 (FTO), or Method 2 (FTO and ITO), was performed to gain an in-depth understanding of the surface composition. The XPS-derived surface quantification and speciation are summarized in Tables S2 and S3 (Supporting Information), and the

complete overview of the survey spectrum and high-resolution regions with the fitted Sn 3d,^[36] Sn 3p, Fe 2p,^[37] In 3p, In 3d, O 1s, C 1s and Zn 2p peaks are presented in Figures S26–S37 (Supporting Information) for each sample. The pH and FeSO_4 concentration in the treatment solutions were varied to further understand how they impact the surface treatment. There are clear differences in the composition and chemical speciation of FTO surfaces after treatment with either ReTreat Method 1 or Method 2. Comparison of the Sn 3d region for untreated FTO, and FTO treated using Method 1 and Method 2 are presented in Figure 4. Both treatment methods lead to the reduction of SnO_2 to SnO and Sn^0 and a simultaneous decrease in the relative amount of oxygen at the surface (Table S2, Supporting Information). Method 1 leads to a larger amount of metallic Sn^0 ($\approx 12\%$), which is attributed to the lower pH, higher reactivity of the solution, and direct contact of Zn powders with the surface. Further comparison of the Fe 2p and Sn 3p regions shows that only Method 1 results in the presence of Fe at the surface of FTO (Figure 4). These observations fall in line with what is shown from the XRD and EDS analysis (Table 1, Figures S2 and S4, Supporting Information). By using peak parameters defined by Biesinger et al. for the Fe 2p region, the speciation of the Fe deposited at the surface is determined to be composed of 60% Fe^{3+} (Fe_2O_3), 36% Fe^{2+} (FeO) and 5% metallic Fe^0 species.^[37] These results indicate that both an iron oxide and one or more intermetallic Fe_xSn_y alloys are formed at the surface. In addition, the XPS analysis reveals that there is a significant amount of residual Zn remaining at the surface of the FTO after Method 1 ($\approx 22\%$), as compared to Method 2 ($< 0.5\%$), see Table S2

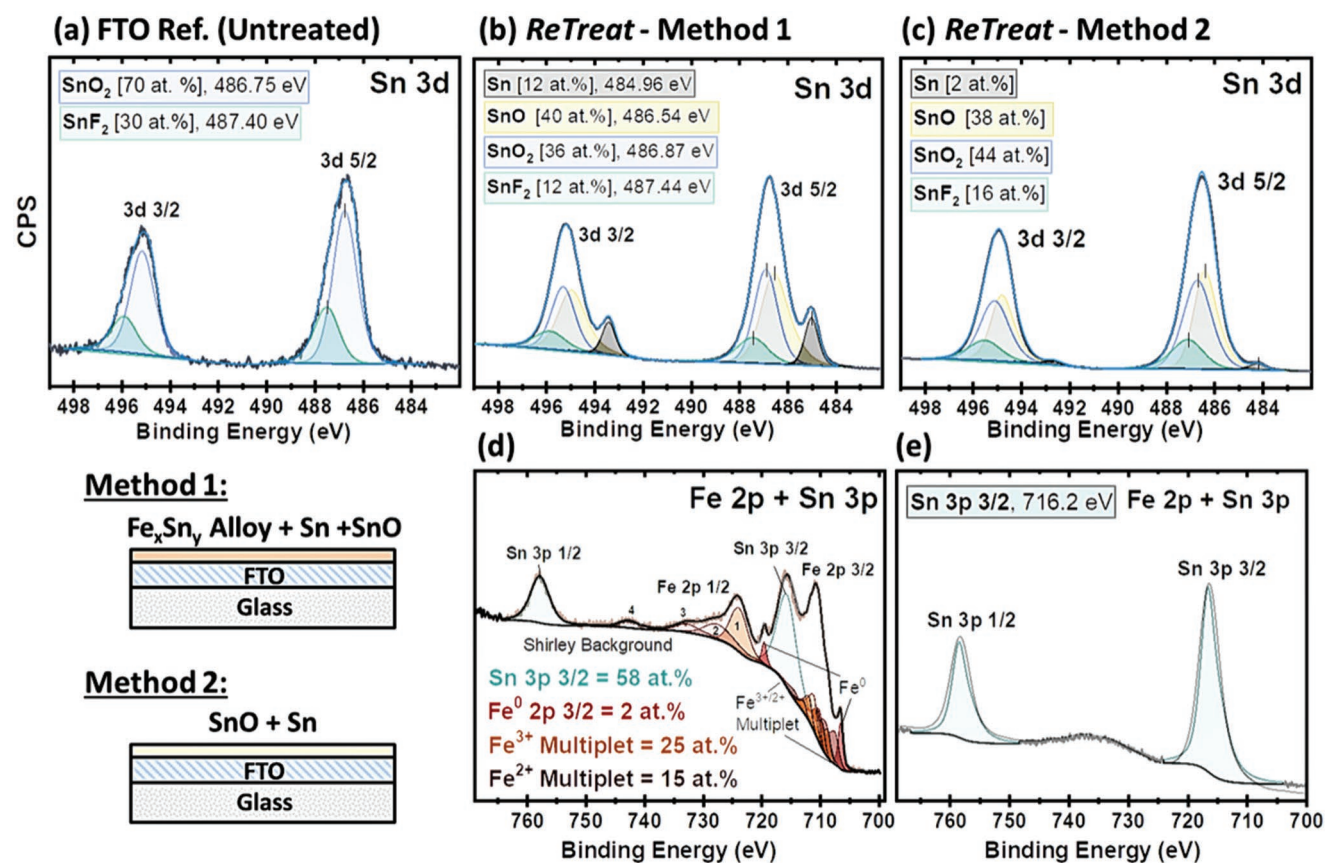


Figure 4. XPS analysis providing high-resolution Sn 3d, Fe 2p, and Sn 3p regions of FTO a) before and after ReTreat using either b,d) Method 1 or c,e) Method 2.

(Supporting Information). As mentioned, Method 1 involves the direct dispersion of Zn powders (reducing agent) onto the TCO surface, leading to a higher amount of Zn^{2+} species available to contaminate the surfaces after treatment and washing. As mentioned, Method 1 involves the direct dispersion of Zn powders (reducing agent) onto the TCO surface, and therefore remains on the surface even after washing with water. From the Zn 2p spectra the peak binding energies of the fitted Zn 2p 3/2 and Zn 2p 1/2 peaks are 1021.86 and 1044.86 eV, respectively. Due to the Zn 2p spectral overlap of peaks for metallic Zn (1021.65 eV) and ZnO/Zn^{2+} (1021.00 eV) species it was not possible to accurately identify and quantify the chemical speciation of the Zn at the surface. The FWHM for the Zn 2p3/2 peak in our analysis of FTO samples treated with method 1 is ≈ 1.54 eV (± 0.05 eV), which agrees well with the value for ZnO/Zn^{2+} species. However, it should be noted that this level of analysis could not be taken as definitive, as there are other factors that may result in the broadening of FWHM. Zn chemical states can also be determined by using the modified Auger parameters for Zn and ZnO. However, in our XPS measurement, the Sn 3d peaks (binding energy ranging from 495 to 484 eV) overlap with the Zn LMM Auger region (binding energy ≈ 501 eV/kinetic energy ≈ 987 eV), which prevents any reliable fitting/analysis of the Zn LMM Auger spectrum (Figure S27, Supporting Information).^[38]

Table S3 (Supporting Information) summarizes the XPS quantification analysis of the ITO samples before and after

ReTreat following Method 2 only. The survey and high-resolution XPS spectra of the untreated ITO films are summarized in Figure S29 (Supporting Information) and the calculated atomic ratio of In:Sn is around 10:1, which is the expected composition of such ITO samples. Comparing the Sn 3d and In 3d spectra of the untreated ITO with treated ITO samples shows that the ReTreat process only reduced the SnO_2 to SnO and Sn, whereas the In_2O_3 does not appear to be reduced by the surface treatment. Both the pH and $FeSO_4$ concentration can significantly modify the reduction rate of SnO_2 and the relative ratio of SnO_2 , SnO, and Sn^0 at the surface (Figure 5). Lowering the pH increases the relative amount of SnO and Sn^0 formed at the surface, and the formation of metallic Sn^0 becomes more favored using more acidic solutions (Figure 5a). A similar trend is observed with increasing $FeSO_4$ concentration (Figure 5b). These data indicate that the pH and $FeSO_4$ concentrations play a significant role in the reaction mechanism and kinetics of the ReTreat processes.

2.5. In situ Optical Transmittance Analysis

We performed in situ optical transmittance analysis to observe the time-dependent optical changes in the FTO and ITO during the different surface treatments. Experiments were designed to understand the influence of pH and $FeSO_4$ concentration in

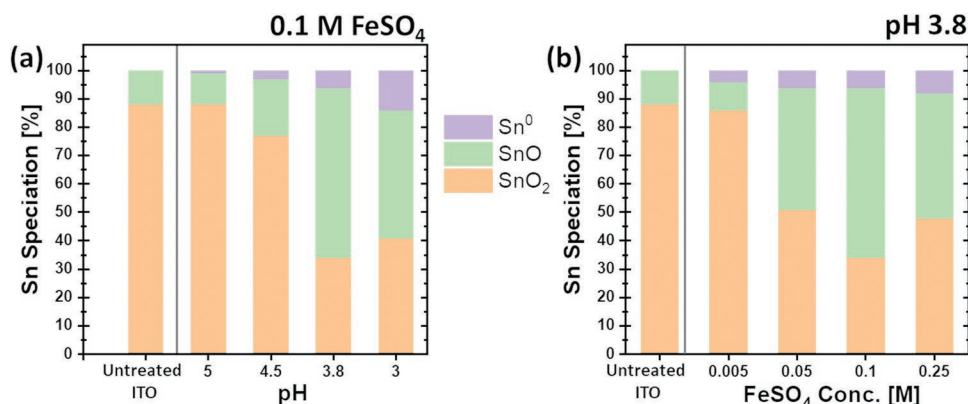


Figure 5. The relative quantities of Sn species determined for the different untreated and treated ITO coated PET samples as derived from the peak fitting of Sn 3d XPS region. a) The influence of the pH of the 0.1 M FeSO₄ ReTreat solutions on the Sn speciation at the surface after treatment using Method 2. b) The influence of the FeSO₄ concentration in pH 3.8 ReTreat solutions on the Sn speciation at the surface after treatment using Method 2.

ReTreat solutions on the reduction rate of TCO surfaces and aimed to exclude the impact of Zn powders. Therefore, only Method 2 is used in situ optical transmittance investigations. As illustrated in **Figure 6**, measurements were conducted by vertically immersing either FTO coated glass or ITO coated PET substrates into a quartz cell containing an “active” ReTreat solution as described in Method 2 (see Figure 1).

A detailed discussion of the transmittance analysis of the “active” ReTreat solutions is also provided in Section S2 of the Supporting Information. In brief, it is found that Fe²⁺ ions are less stable to oxidation in aqueous solutions with pH > 3.8, which corresponds with the previously reported pH-dependent stabilities of Fe²⁺ and Fe³⁺ ions.^[39] By adding zinc powders to the FeSO₄ solutions oxidized Fe³⁺ ions are reduced to Fe²⁺ and the ReTreat solution is considered to be in the “active” state (Method 2). The change in the transmittance spectrum following the activation treatment is shown in **Figure 7a**.

For the in situ transmittance measurements, the TCO samples are placed in the active ReTreat solution with either different

pH or FeSO₄ concentrations and the reduction rate of the TCO is monitored by the time dependent decrease or changes in the relative transmittance spectra. The initial transmittance spectrum of the TCO and the respective ReTreat solution is measured and assigned to time zero (t₀) (Figure 7b,c). Then subsequent transmittance spectra were measured continuously with an integration time of 2s and for the duration of the surface treatment (~20 min). To monitor only the changes in the TCO absorption, the transmittance spectrum of the quartz cell plus the respective ReTreat solution and the TCO coated substrate at t₀ was used as the reference spectrum (I₀), as shown in Figure 7c.

As an example, Figure 7c shows the time-dependent transmittance data of an FTO coated glass sample in an active pH 3, 0.1 M FeSO₄ ReTreat solution. It is observed that as surface reaction proceeds, the TCO transmittance decreases over time. It is apparent from the photographic image in Figure 7c that a brown coating forms at the surface after analysis, which is attributed to the formation of SnO and Sn as identified from XPS.

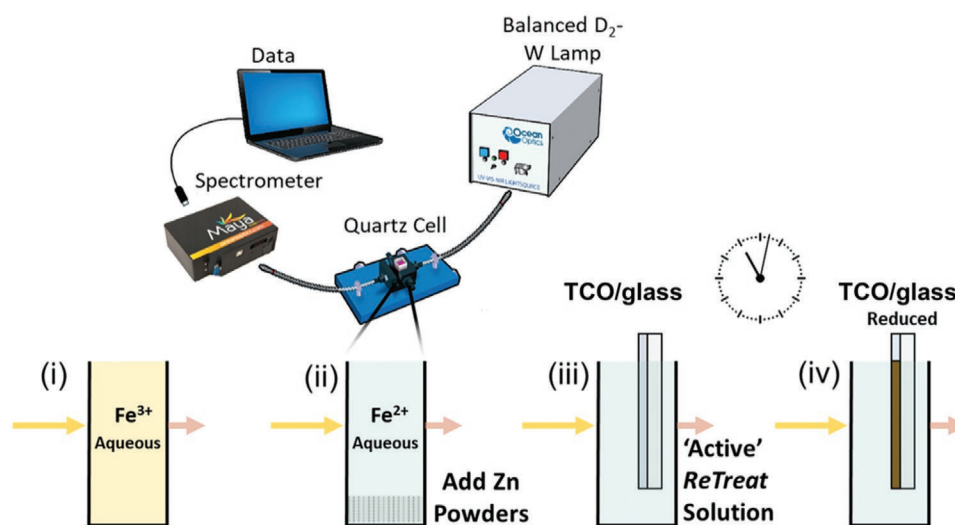


Figure 6. Illustration of the in situ spectrochemistry analysis setup and the steps for measuring the transmittance spectra of the ReTreat solution i) before and ii) after activation. iii, iv) represent the procedure to measure the time dependent transmittance spectra of the Sn-containing TCOs during surface treatment.

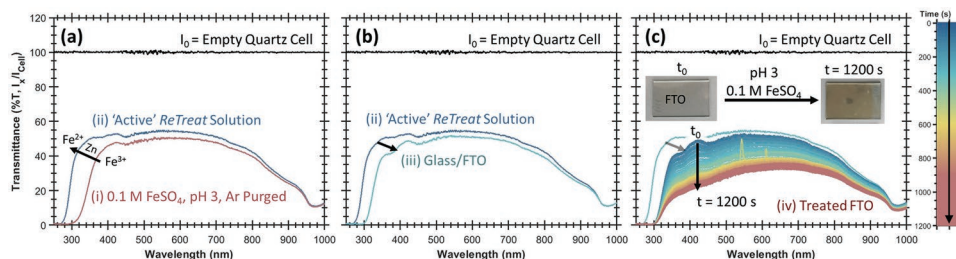


Figure 7. a–c) Examples of the transmittance spectra measured at each step during preparation and activation of the ReTreat solution following Method 2. Here we present the solution consisting of 0.1 M FeSO_4 and 1.0 M glycine at pH 3. Step (i) to (ii) shows the transmittance of the solution before and after the addition and filtration of 0.1 M of Zn powders to generate an “active” ReTreat solution. Step (iii) to (iv) shows the in situ transmittance measurements for a FTO coated glass substrates during surface treatment. All in situ optical transmittance measurements followed the same procedure and were carried out at room temperature and without stirring.

The surface reduction rates and formation rate of SnO and Sn are derived from in situ optical transmittance analysis using the method described in the supporting information (Section S3, Supporting Information). As a summary, the time dependent transmittance values at two discrete wavelengths are used to determine the absorbance of both SnO and Sn at 400 nm and just Sn at 900 nm. From these absorbance values, the relative thickness (d) of Sn and SnO can be calculated. **Figure 8** shows the curves for the calculated time dependent thicknesses of SnO and Sn fractions during surface treatment of FTO in a pH 3 and 0.1 M FeSO_4 ReTreat solution. At the start of the surface treatment, there is a fast generation of SnO and Sn and the respective film thicknesses increase linearly with time, indicating that the initial reaction rate (r_{initial}) is relatively constant. As the surface treatment reaction proceeds the generation of SnO and Sn slows down and eventually ceases. To gain an understanding of the reaction kinetics, the gradient of the initial linear region was determined and respective initial growth rates for SnO and Sn species (nm s^{-1}) were calculated. Using reported densities of SnO and Sn, the initial growth rates were then converted to an instantaneous reaction rate (moles of SnO, Sn or electrons $\text{m}^{-2} \text{s}^{-1}$) and used as a comparative measure of the reaction kinetics, as shown in Table S4 (Supporting Information). For more details, see Section S3 of the Supporting Information

2.6. The Impact of TCO Type, pH and FeSO_4 Concentration on the ReTreat Reaction Rate and Sn Speciation

From Table S4 (Supporting Information), it is initially clear that the FTO coated glass samples exhibit lower reduction rates compared to ITO coated PET samples. The slower reaction rate means only a small fraction of the FTO film is reduced when using ReTreat Method 2. The FTO is reduced at a maximum rate of 0.041 nm s^{-1} when using a pH 3 solution containing 0.1 M FeSO_4 (Figure 8). Based on this initial rate, the chemical reduction process would reduce $\approx 50 \text{ nm}$ of the FTO after 1200 seconds. However, as noted the reaction rate decreases with treatment time and begins to plateau after 1000 s. As a result, only a $\approx 35 \text{ nm}$ layer is reduced after 1200 s of treatment and is equivalent to less than 10% of the overall thickness of the 400 nm FTO film (Figure 8b). The decrease in reduction rate with extended treatment time is attributed to the consumption of reactive Fe^{2+} ions close to the TCO surface (Figure S41, Supporting Information), and/or the limited penetration depth of the treatment solution, which is influenced by the pH (Figure S42, Supporting Information).

As shown in **Figure 9a**, the reduction rates for both ITO and FTO increase as the pH decreases. However, the ITO coated PET samples display faster reaction rates compared to the FTO on glass (Table S4, Supporting Information). The differences in reaction rates between FTO on glass and ITO on PET can

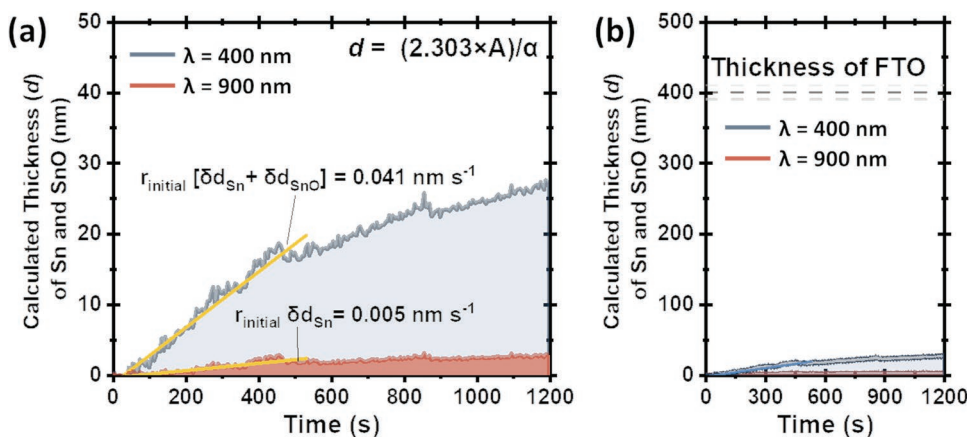


Figure 8. a) The calculated time dependent thicknesses of Sn and SnO generated at the surface of the FTO films during in situ optical transmittance analysis using pH 3, 0.1 M FeSO_4 active ReTreat solutions. b) The same data scaled to the relative thickness of the FTO film ($\approx 400 \text{ nm}$).

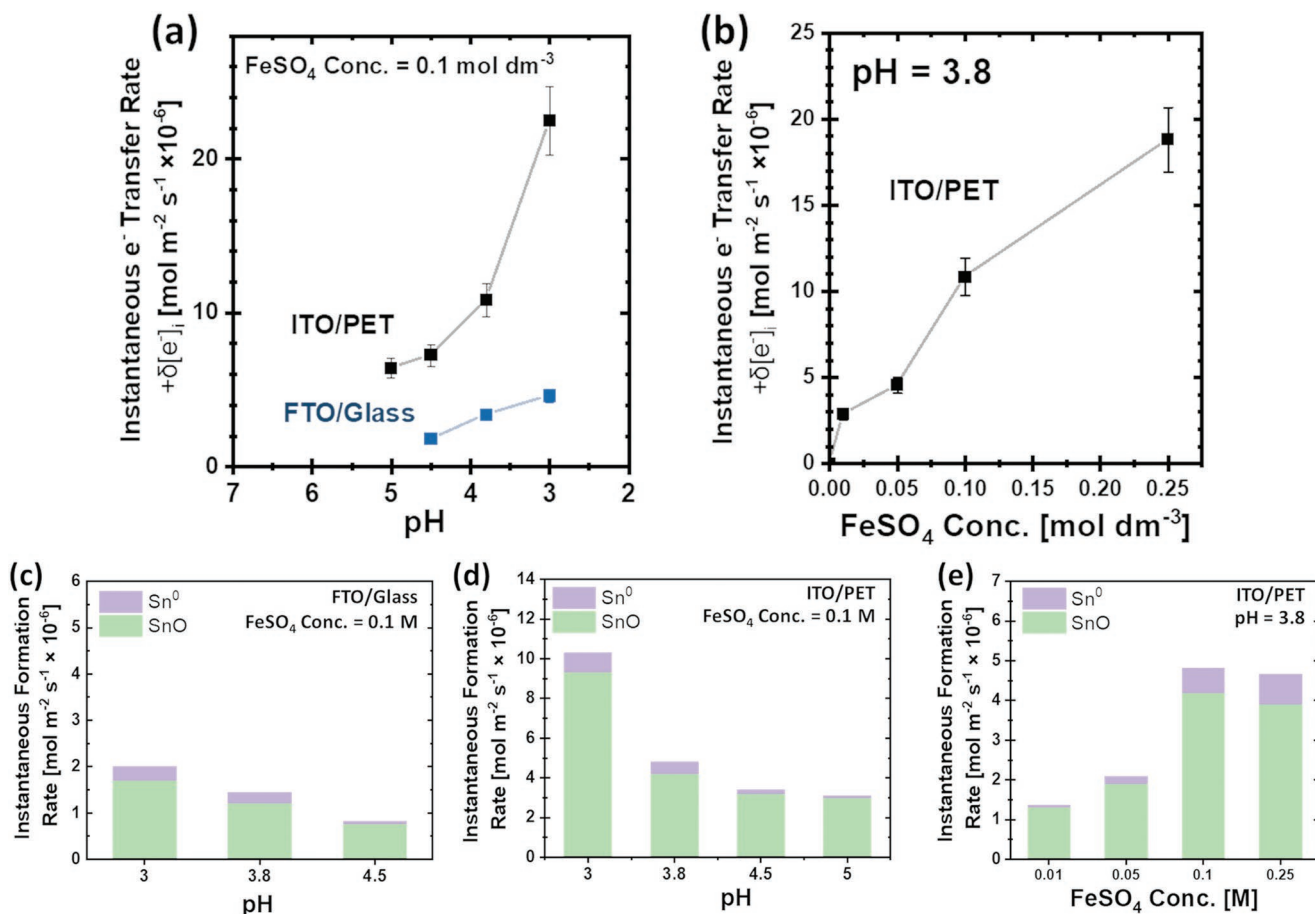


Figure 9. The pH and FeSO₄ dependent a,b) instantaneous electron transfer rate (e⁻ mol m⁻² s⁻¹) and c,d, e) SnO and Sn formation rate (mol m⁻² s⁻¹) determined from in situ optical transmittance measurements of surface treated FTO on glass and ITO on PET.

be attributed to their surface area, roughness, degree of crystallinity, and relative chemical stability. ITO grown on PET is less crystalline as lower processing temperatures (200 °C) are used to fabricate such substrates.^[40] Using equivalent ReTreat solutions with a pH of 3 and 0.1 M FeSO₄, the initial reaction rate is calculated to be 0.21 nm s⁻¹, under the assumption that the 10% SnO₂ in the ITO film is uniformly distributed and is the only component reduced in the ITO film. A typical ITO film on PET has an average thickness of 100 nm, and at this high reaction rate, it is expected that the entire SnO₂ content within the ITO film will be reduced to either SnO or Sn within 60 s (Figure S42, Supporting Information). Sheet resistance measurements reveal that the ITO becomes highly resistive after 20 s of treatment and SEM images of the ITO films after different treatment times indicate that the films corrode and become discontinuous (Figure S38, Supporting Information). It is speculated that the corrosion is due to the dissolution of In₂O₃ in pH 3 solutions combined with the fast reduction of SnO₂, which may be attributed to the lower crystallinity of the ITO on PET compared to the FTO films on glass.

Figure 9 indicates that increasing the pH from 3 to 5 leads to a decrease in the initial reduction rates, and Figure S42 (Supporting Information) suggests that the maximum depth of surface reduction becomes more limited at higher pH.

Interestingly at pH 3.8, the initial reduction rate of ITO also has a linear dependence on the FeSO₄ concentration between 0.01 and 0.25 M (Figure 9b). However, with extended treatment times the reaction rate decreases, and eventually terminates (Figure S41, Supporting Information), thus limiting the total amount of SnO₂ that can be reduced. As is the case with lowering the pH, higher concentrations of FeSO₄ can also be used to limit treatment depth and inhibit excessive etching of Sn-containing TCOs during surface treatment.

The in situ transmittance analysis also reveals that the pH and FeSO₄ concentration influences the relative formation rates of the SnO and Sn surface species. As seen from Figure 9c,d, with decreasing pH the relative initial formation rate for metallic Sn increases. For example, for the treatment of an FTO film on glass using a 0.1 M FeSO₄ solution, the instantaneous formation rate for Sn is only 0.06 mol m⁻² s⁻¹ at pH 4.5, which increases to 0.35 mol m⁻² s⁻¹ at pH 3. Similarly higher concentrations of FeSO₄ also increase the relative formation rate of metallic Sn, as observed in Figure 9e. These results are consistent with the ex situ XPS surface analysis (Figure 5) and provide further evidence that the concentration of H⁺ and Fe²⁺ influences the reduction potential of the treatment bath and affects the electron transfer rate to the surface.

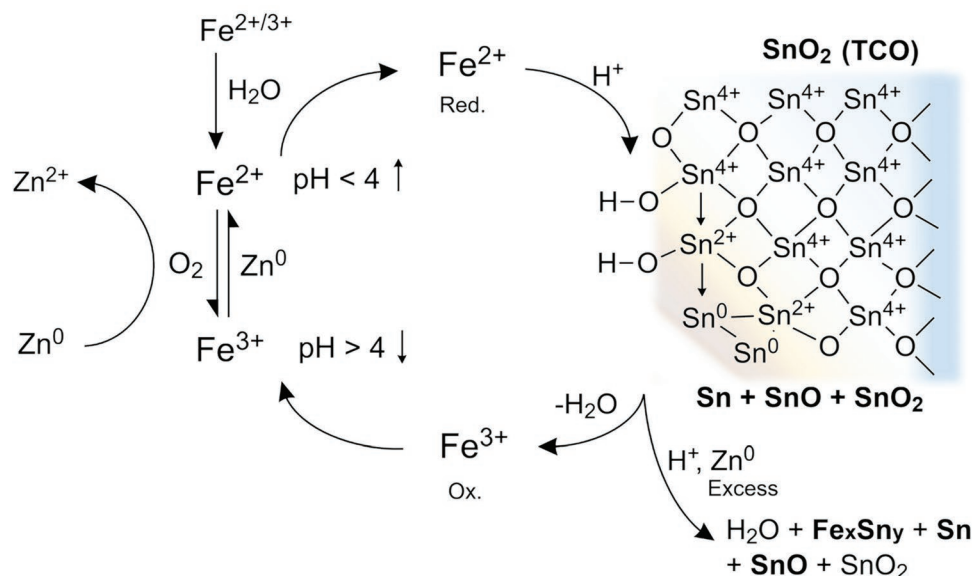
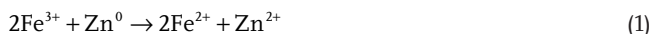


Figure 10. A heuristic representation of the heterogeneous surface reaction between Sn-containing TCOs and the reagents within the aqueous ReTreat solutions.

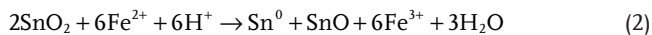
By drawing together materials characterization data from XRD and XPS analysis with the results derived from in situ transmittance measurements, we propose a heuristic description of the heterogeneous reaction mechanism between Sn-containing TCOs and the ReTreat surface treatment solutions (**Figure 10**). In summary, the pH of the treatment solutions determines the oxidative stability of Fe^{2+} ions. During the “activation” step in Method 2, a slurry of Zn powder reduces any Fe^{3+} ions that were oxidized from Fe^{2+} by residual dissolved oxygen. After filtering the Zn, the “active” ReTreat solutions consist of a high concentration of Fe^{2+} ions which mediate the reduction of only the SnO_2 during surface treatment. The pH and concentration of Fe^{2+} ions determine the initial reduction rate of SnO_2 and can modify the reduction depth as well as the relative formation rate of reduced Sn species (i.e., SnO or Sn).

A summary of the principal reactions within the ReTreat process is provided below.

Reduction of Fe^{3+} ions by Zn:

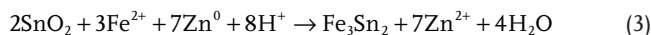


The proton assisted reduction of SnO_2 by Fe^{2+} ions:



Method 1 of the ReTreat process uses solutions with higher acidity ($\approx \text{pH } 3$). In this case, the Fe^{2+} ions remain stable to oxidation. For this surface treatment method, there is a direct contact between the Zn powders and SnO_2 (TCO) surfaces, therefore the Zn reducing agents mediate the reduction of both the Fe^{2+} ions and SnO_2 to form an intermetallic Fe_xSn_y alloys at the surface in combination with SnO and metallic Sn. Furthermore, it is demonstrated that the initial concentration of FeSO_4 can influence the stoichiometry of the Fe_xSn_y alloy formed. The proposed reaction for solutions containing a low concentration

of FeSO_4 ($\approx 0.1 \text{ M}$) and result in Fe_3Sn_2 alloy formation is written below:



In addition to the above reactions, the Zn powders react with the acidic aqueous solutions to form hydrogen gas. This side reaction becomes more predominant at lower pH.

3. Conclusions

In conclusion, we provide a comprehensive description of a novel surface treatment process (ReTreat) for the selective reduction of Sn-containing TCO surfaces. The process uses aqueous glycine buffered solutions consisting of an Fe^{2+} salt (FeSO_4) and Zn powders as a reducing agent, which can be easily prepared and used to pre-treat thin films of Sn-containing TCOs prior to electroplating. The surface treatment significantly improves the uniformity, selectivity, and adhesion of electroplated metal films (incl. Au, Ni, and Ag) on commercial FTO-coated glass and ITO-coated PET. It is demonstrated that ReTreat is compatible with several masking materials, and a wide range of masking patterns and geometries are presented. The electroplated Au and Ni films demonstrate excellent film quality, and fulfill a variety of standardized tests for adhesion, thermal stability (IR Reflow and air annealing) and electronic reliability (HAST). Such level of durability permits the use of this technology in a variety of high temperature fabrication processes. Furthermore, the Au films electroplated on treated ITO coated PET were highly tolerant to bending and folding, offering applications in flexible electronics.

Combining XRD and XPS analysis of the FTO and ITO after surface treatment reveals that the ReTreat process reduces the SnO_2 to a mixture of SnO and metallic Sn. Fe_xSn_y alloys are

also formed under highly acidic treatment conditions (\approx pH 3) and when Zn powders are in direct contact with the surface of FTO. The stoichiometry of the Fe_xSn_y alloys is shown to be influenced by the concentration of FeSO_4 in the treatment solution.

In situ optical transmittance analysis during surface treatment of FTO and ITO was used to determine the ReTreat reaction mechanism and the reaction kinetics. The pH and FeSO_4 concentration in the treatment solution, as well as the type of Sn-containing TCO can impact the reaction rate of the surface treatment process, and the concentration of reagents can be modified to control the penetration depth of the chemical reduction. This detailed assessment of the ReTreat surface treatment process provides the necessary knowledge for its future implementation in the fabrication of reliable interfaces between TCOs and metals. This innovative process has strong industrial applicability and a potential value in a broad range of scientific and engineering fields, where it is expected to serve as a customary treatment step for Sn-containing TCOs prior to the electrodeposition of metallic coatings.

4. Experimental Section

Surface Treatment and Masking of FTO on Glass and ITO on PET: FTO coated glass substrates (Pilkington, TEC 15, $\approx 13 \Omega \text{ sq}^{-1}$) and ITO coated PET substrates (Merck, $\approx 60 \Omega \text{ sq}^{-1}$) were cleaned using soapy water (10 vol% Triton-X), Milli Q water (18.2 M Ω cm), ethanol, and then dried under a flow of compressed N_2 . The substrates were masked with either Kapton tape, polymethylmethacrylate (PMMA) photoresist, or permanent marker (Staedtler).

For the reductive surface treatment (ReTreat), two methods were developed for FTO coated glass (Method 1) and ITO coated PET substrates (Method 2).

Method 1: For Method 1 of the surface treatment process, a pH 3.8, 1.0 M glycine ($\geq 99\%$; Aldrich) buffered solution was prepared by adjusting the pH with 0.1 M H_2SO_4 and 0.1 M NaOH. The solution was then purged with Ar gas (60 sccm) for 30 min. An aqueous 0.1 M solution of $\text{FeSO}_4 \cdot 7\text{H}_2\text{O}$ ($\geq 99\%$; Aldrich) was added to the glycine solution. The solutions were then transferred to a glass treatment bath. FTO coated glass substrates (with or without mask) were placed face upwards in the treatment solution and soaked for a duration of 30 s. Zn powders (mesh 100, $\geq 97\%$ Fisher Scientific) were then uniformly dispersed over the surface of the FTO and allowed to react for 10 min, during which hydrogen bubbles evolved. It is important to note that the particle/mesh size makes a significant impact, and it is advised to use Zn powders with a mesh size >100 , which is equivalent to particle size of $< 150 \mu\text{m}$. After this time, the treatment bath was sonicated to remove bubbles and Zn powders from the FTO surface. The FTO substrates were then washed with a fast jet of deionized water and dried with N_2 gas. After treatment, a shiny adherent intermetallic film was visible on the surface of the exposed regions of the FTO (see Video S1, Supporting Information).

Method 2: In this method, the ReTreat solutions require an initial "activation-step" prior to the actual TCO surface treatment. In the activation step, Zn powders are added into a stirred pH 3, 0.1 M FeSO_4 solution to form a slurry. Resultantly Fe^{3+} ions in solution are reduced by Zn to Fe^{2+} causing a visible color change from pale orange to pale blue. The Zn powders are then removed by centrifugation, decantation, and filtration (Whatman Grade 1:11 μm). The ReTreat solution is then considered to be in the "active" state. For surface treatment, ITO or FTO coated substrates are immersed in the active ReTreat solution and allowed to react using an optimized time of 2 min for ITO on PET and 40 min for FTO on glass. After surface treatment, the TCOs are removed from the solution and washed with a fast jet of deionized water and dried with pressurized air or N_2 gas. After treatment, the masking material is

removed, and within the treated regions a brown film is visible on the surface of the TCO.

Electrodeposition of Metal Films: Contacts to the FTO or ITO were made by painting a thin line of silver paste along the top edge of the substrate and contacting with a crocodile clip. The electrochemical depositions were performed in a three-electrode electrochemical cell using a VersaSTAT 3 potentiostat/galvanostat (Ametek). The pre-treated masked TCO functioned as the working electrode and a Pt coated Ti mesh served as the counter electrode and were placed face to face with a distance ≈ 5 cm. An Ag/AgCl (XR300, saturated KCl, Radiometer Analytical) was used as a reference electrode.

Electrochemical deposition of Au, Ni, and Ag was performed under galvanostatic conditions. For electroplating onto treated FTO a current density of -5 mA cm^{-2} for Au and Ag deposition or -10 mA cm^{-2} for Ni deposition was used, with a duration of either 120 s or 900 s to produce metallic films with a thickness of $200 \pm 20 \text{ nm}$ or $1.0 \pm 0.1 \mu\text{m}$, respectively. For electrodeposition onto treated ITO-coated PET, a lower current density of -0.5 mA cm^{-2} (Au and Ag) or -1.0 mA cm^{-2} (Ni) was used with a longer deposition time of 1200 s. The differences in the optimized deposition procedures were attributed to the different sheet resistances for FTO on glass (TEC 15, $\approx 13 \Omega \text{ sq}^{-1}$) and ITO on PET ($\approx 60 \Omega \text{ sq}^{-1}$).

For Au electroplating, a commercial acidic and cyanide-based bright gold plating bath 750 SC (Wieland Edelmetalle GmbH) was used. For Ni electroplating, the electrolyte was prepared from 1.14 M $\text{NiSO}_4 \cdot 7\text{H}_2\text{O}$ ($\geq 98\%$, Aldrich), 0.16 M $\text{NiCl}_2 \cdot 6\text{H}_2\text{O}$ ($\geq 98\%$, Aldrich), and 0.73 M H_3BO_3 ($\geq 99.5\%$, Aldrich) in deionized water ($>18 \text{ M}\Omega \text{ cm}$). For Ag electroplating, the plating bath was purchased from a commercial supplier (Wilaplat) and consisted of 30 g L^{-1} of Ag and 120 g L^{-1} of cyanide salts. During all electrochemical depositions, the electrolyte was heated to 40 °C and stirred. After the deposition, the masking material was removed and substrates were ultrasonically cleaned in deionized water, acetone, and ethanol for 60 s each, and then dried under a fast jet of N_2 . The sheet resistances of the TCOs after treatments and the electroplated metal were measured using a 4D Inc. automatic 4-point probe meter, Model 280I Series.

Standardized Testing: Adhesion tests were conducted following the Elcometer 107 crosshatch and tape test method and the results compared to tabulated ISO classifications. Manual bending tests of Au coatings on treated ITO/PET substrates were performed for 250 cycles with a fold radius $< 1 \text{ mm}$.

To simulate the operating conditions used within the electronic printed circuit board industry and as a measure of thermal stability, electroplated samples were subjected to thermal infrared reflow annealing using a REHM Compact Nitro B2100/460 Reflow oven. The temperature versus time profile for the annealing is presented in Figure S24 (Supporting Information) and the samples were subjected to consecutive annealing cycles initially in N_2 gas (6 cycles) and O_2 gas (2 cycles). Samples were then examined for electrical conductivity, delamination, and adhesion.

Standardized highly accelerated stress testing (HAST) was performed using an Espec EHS-221 M system and in air with a humidity of 85%, a temperature of 130 °C and duration for 95 h (type U IEC conditions). After IR Reflow and HAST testing, all samples were examined and assessed for electrical conductivity and sheet resistance, delamination, and adhesion.

Materials Characterization: GIXRD measurements were performed using a Bruker D8 diffractometer with Cu $K\alpha$ radiation at 40 kV and 40 mA. Scanning electron microscopy (SEM) images and energy-dispersive X-ray spectroscopy (EDS) spectra were obtained using a LEO GEMINI 1530 with a Thermo Fisher EDS detector, with a 15 keV acceleration voltage.

X-ray photoemission spectroscopy (XPS) was measured in a home-built ultrahigh vacuum system at $< 10^{-8}$ mbar. XPS was performed with a monochromatic Al $K\alpha$ X-ray source (1486.74 eV) using a SPECS FOCUS 500 X-ray monochromator and a SPECS PHOIBOS 100 hemispherical analyzer. The source-to-analyzer angle was set at 54°. All high-resolution spectra were measured using a pass energy and step size of 10 and 0.05 eV, respectively. CasaXPS was used for the data processing and

peak fitting. To calibrate the peak position, the C 1s peak was fitted to the aliphatic carbon reference of 284.8 eV and the other peak positions were adjusted accordingly. A Shirley background was used for all peak models. The elemental ratios were determined from the total peak areas of the O 1s, Sn 3d_{5/2}, (In 3d_{5/2} in the ITO samples), and deconvolution of the Sn 3p_{3/2} and Fe 2p_{3/2} peaks, divided by the product of the respective relative sensitivity factors, transmittance function of the analyzer (T), and the energy-dependent inelastic mean free path (MSF). The relative area calculated from a fitted peak model for the Sn 3p_{3/2} and Fe 2p_{3/2} region was used to determine the ratio of Fe³⁺, Fe²⁺ and Fe⁰.^[37]

In situ Transmittance Measurements: In situ transmittance measurements of the TCOs during reductive surface treatment were performed using a home-built system. A transparent cell constructed of fused silica (quartz) was placed in black painted cabinet. The cell was illuminated with a light source provided by a balanced deuterium-halogen lamp (DH-2000-BAL, Ocean Optics) channeled through a solarization resistant optical fiber/collimator assembly, which generated a parallel beam of light with a diameter of ≈5 mm through the cell. The transmitted light was then collected by another optical fiber/collimator assembly and delivered to a spectrometer (MAYA 2000-Pro, Ocean Optics) with a 200–1100 nm detection range. The transmittance spectra of both the cell without and with the active ReTreat solution was recorded. The TCO sample was then placed in the treatment solution in the center of the cell with the TCO surface facing perpendicular toward the illumination beam. The light intensity/transmittance spectra were measured continuously with an integration time of 2 s and for a duration of 1200 s. The time-dependent spectra/transmittance data was post-processed and plotted using a MATLAB code, which automatically identified the spectra for the empty cell, cell with the active ReTreat solution and the spectra of the TCO during surface treatment from t_0 to t_x . The time-dependent transmittance was converted to absorbance and used to calculate the respective thicknesses of Sn and SnO at selected wavelengths (400 and 900 nm).

Supporting Information

Supporting Information is available from the Wiley Online Library or from the authors.

Acknowledgements

The authors acknowledge Dr Tatjana Königsmann at Atotech GmbH for conducting the infrared (IR) Reflow assessment and highly accelerated stress testing (HAST). Dr Felix Hermerschmidt (Humboldt-Universität Berlin) is acknowledged for performing the Elcometer Cross-hatch adhesion tests following ISO and ASTM protocols. Preliminary experiments for this work were conducted as part of the PECDEMO project, which was funded by Europe's Fuel Cell and Hydrogen Joint Undertaking (2014-2017; Grant Agreement No. 621252).

Open access funding enabled and organized by Projekt DEAL.

Conflict of Interest

Three of the authors (I.Y.A., F.F.A., and R.V.D.K.) are named as inventors of international patent application WO 2019/052598 and German Patent Application DE 10 2017 121 228 A1, which are held by Helmholtz-Zentrum Berlin für Materialien und Energie GmbH. The subject of the manuscript related to surface treatment of FTO and ITO prior electroplating covers the scope of the patent application.

Data Availability Statement

The data that support the findings of this study are available from the corresponding author upon reasonable request.

Keywords

adhesion promoters, electroplating, intermetallic layers, surface treatments, transparent conducting oxides

Received: July 22, 2022

Revised: September 27, 2022

Published online: October 26, 2022

- [1] a) D. S. Ginley, C. Bright, *MRS Bull.* **2011**, 25, 15; b) M.-I. Baraton, *MRS Proc.* **2011**, 1209, 1209.
- [2] R. G. Gordon, *MRS Bull.* **2011**, 25, 52.
- [3] S. J. Laverty, H. Feng, P. Maguire, *J. Electrochem. Soc.* **1997**, 144, 2165.
- [4] C. M. Lampert, *Sol. Energy Mater. Sol. Cells* **2003**, 76, 489.
- [5] C. Ros, T. Andreu, J. R. Morante, *J. Mater. Chem. A* **2020**, 8, 10625.
- [6] a) J. Yang, W. Liu, L. Dong, Y. Li, C. Li, H. Zhao, *Appl. Surf. Sci.* **2011**, 257, 10499; b) R. Gottesman, A. Song, I. Levine, M. Krause, A. T. M. N. Islam, D. Abou-Ras, T. Dittrich, R. van de Krol, A. Chemseddine, *Adv. Funct. Mater.* **2020**, 30, 1910832; c) S. Gahlawat, I. Y. Ahmet, P. Schnell, I. Levine, S. Zhang, P. P. Ingole, F. F. Abdi, *Chem. Mater.* **2022**, 34, 4320; d) A. Way, J. Luke, A. D. Evans, Z. Li, J.-S. Kim, J. R. Durrant, H. K. H. Lee, W. C. Tsoi, *AIP Adv.* **2019**, 9, 085220; e) Pilkington; Solaronix, **2020**, <https://www.pilkington.com/en/global/products/product-categories/solar-energy/nsg-tec-for-solar-applications> (accessed: October 2022).
- [7] C.-W. Yang, J.-W. Park, *Surf. Coat. Technol.* **2010**, 204, 2761.
- [8] R. B. H. Tahar, T. Ban, Y. Ohya, Y. Takahashi, *J. Appl. Phys.* **1998**, 83, 2631.
- [9] a) M. M. Hamasha, T. Dhakal, K. Alzoubi, S. Albahri, A. Qasaimeh, S. Lu, C. R. Westgate, *J. Disp. Technol.* **2012**, 8, 385; b) M. Nasr Saleh, G. Lubineau, *Sol. Energy Mater. Sol. Cells* **2014**, 130, 199; c) M. Supplies; d) A. Andersson, N. Johansson, P. Bröms, N. Yu, D. Lupo, W. R. Salaneck, *Adv. Mater.* **1998**, 10, 859; e) M. A. Green, *Prog. Photovoltaics* **2009**, 17, 347.
- [10] a) H. Duan, J. Wang, L. Liu, Q. Huang, J. Li, *Prog. Photovoltaics* **2016**, 24, 83; b) K. Zhang, Y. Wu, W. Wang, B. Li, Y. Zhang, T. Zuo, *Resour., Conserv. Recycl.* **2015**, 104, 276; c) M. Lokanc, R. Eggert, M. Redlinger, *National Renewable Energy Laboratory (NREL), Golden, CO (United States), United States* **2015**, Medium: ED; Size: 90 p, <https://www.nrel.gov/docs/fy16osti/62409.pdf> (accessed: October 2022).
- [11] a) D. S. Hecht, L. Hu, G. Irvin, *Adv. Mater.* **2011**, 23, 1482; b) A. Kay, M. Grätzel, *Sol. Energy Mater. Sol. Cells* **1996**, 44, 99; c) X. Yao, D. Wang, X. Zhao, S. Ma, P. S. Bassi, G. Yang, W. Chen, Z. Chen, T. Sritharan, *Energy Technol.* **2018**, 6, 100.
- [12] P. C. Andricacos, C. Uzoh, J. O. Dukovic, J. Horkans, H. Deligianni, *IBM J. Res. Dev.* **1998**, 42, 567.
- [13] a) A. Joi, K. Venkatraman, K.-C. Tso, D. Dictus, Y. Dordi, P.-W. Wu, C.-W. Pao, R. Akolkar, *ECS J. Solid State Sci. Technol.* **2019**, 8, P516; b) S. J. Laverty, P. D. Maguire, *J. Electrochem. Soc.* **2000**, 147, 772.
- [14] a) S. Kim, H. Lee, K. Ji, E. Youngjoo, J. Choi, S. Ahn, *WO/2010/058976A2*, **2010**; b) W. J. Lee, P. S. Shinde, G. H. Go, E. Ramasamy, *Int. J. Hydrogen Energy* **2011**, 36, 5262.
- [15] M. Barr, I. Millard, R. Molaro, R. Pandey, *WO/2018/094259A1*, **2020**.
- [16] I. Y. Ahmet, Y. Ma, J.-W. Jang, T. Henschel, B. Stannowski, T. Lopes, A. Vilanova, A. Mendes, F. F. Abdi, R. van de Krol, *Sustainable Energy Fuels* **2019**, 3, 2366.
- [17] B. Y. Ahn, E. B. Duoss, M. J. Motala, X. Guo, S.-I. Park, Y. Xiong, J. Yoon, R. G. Nuzzo, J. A. Rogers, J. A. Lewis, *Science* **2009**, 323, 1590.

- [18] M. Schreier, F. Héroguel, L. Steier, S. Ahmad, J. S. Luterbacher, M. T. Mayer, J. Luo, M. Grätzel, *Nat. Energy* **2017**, *2*, 17087.
- [19] T. Ohmi, T. Saito, M. Otsuki, T. Shibata, T. Nitta, *J. Electrochem. Soc.* **1991**, *138*, 1089.
- [20] a) J. Suikkola, T. Björninen, M. Mosallaei, T. Kankkunen, P. Iso-Ketola, L. Ukkonen, J. Vanhala, M. Mäntysalo, *Sci. Rep.* **2016**, *6*, 25784; b) A. Al-Ashouri, E. Köhnen, B. Li, A. Magomedov, H. Hempel, P. Caprioglio, J. A. Márquez, A. B. M. Vilches, E. Kasparavicius, J. A. Smith, N. Phung, D. Menzel, M. Grischek, L. Kegelmann, D. Skroblin, C. Gollwitzer, T. Malinauskas, M. Jošt, G. Matič, B. Rech, R. Schlatmann, M. Topič, L. Korte, A. Abate, B. Stannowski, D. Neher, M. Stolterfoht, T. Unold, V. Getautis, S. Albrecht, *Science* **2020**, *370*, 1300; c) B. A. Kamino, B. Paviet-Salomon, S.-J. Moon, N. Badel, J. Levrat, G. Christmann, A. Walter, A. Faes, L. Ding, J. J. Diaz Leon, A. Paracchino, M. Despeisse, C. Ballif, S. Nicolay, *ACS Appl. Energy Mater.* **2019**, *2*, 3815.
- [21] a) S. Lopatin, J. O. Dukovic, D. Eaglesham, N. Y. Kovarsky, R. Bachrach, J. Busch, C. Gay, WO/2008/070528A3, **2008**; b) M. Merschky, F. Michalik, M. Thoms, R. Taylor, D. Reinosococina, S. Hotz, T. Bernhard, A. Peter, S. Zarwell, F. Bruening, P. Brooks, "Vitre Coat GI-Employing Metal Oxide Adhesion Layer and Wet Chemical Cu Metallization for Fine Line Pattern Formation on Glass", **2019**, <https://www.atotech.com>; c) O. Schultzwittmann, D. Crafts, D. Deceuster, A. Turner, WO/2012/030407A1, **2012**; d) P. C. Andricacos, *Electrochem. Soc. Interface* **1999**, *8*, 32; e) S. Hirsch, C. Rosenstein, *Met. Finish.* **1999**, *97*, 443; f) S. Hirsch, C. Rosenstein, *Met. Finish.* **2001**, *99*, 305; g) A. Mashreghi, H. Zare, *Curr. Appl. Phys.* **2016**, *16*, 599; h) A. G. Ricciardulli, S. Yang, G.-J. A. H. Wetzelaer, X. Feng, P. W. M. Blom, *Adv. Funct. Mater.* **2018**, *28*, 1706010; i) C.-L. Kim, C.-W. Jung, Y.-J. Oh, D.-E. Kim, *NPG Asia Mater.* **2017**, *9*, e438.
- [22] M. Li, W.-W. Zuo, A. G. Ricciardulli, Y.-G. Yang, Y.-H. Liu, Q. Wang, K.-L. Wang, G.-X. Li, M. Saliba, D. Di Girolamo, A. Abate, Z.-K. Wang, *Adv. Mater.* **2020**, *32*, 2003422.
- [23] a) Y.-H. Liu, J.-L. Xu, S. Shen, X.-L. Cai, L.-S. Chen, S.-D. Wang, *J. Mater. Chem. A* **2017**, *5*, 9032; b) Y.-H. Liu, J.-L. Xu, X. Gao, Y.-L. Sun, J.-J. Lv, S. Shen, L.-S. Chen, S.-D. Wang, *Energy Environ. Sci.* **2017**, *10*, 2534.
- [24] a) H. Su, M. Zhang, Y.-H. Chang, P. Zhai, N. Y. Hau, Y.-T. Huang, C. Liu, A. K. Soh, S.-P. Feng, *ACS Appl. Mater. Interfaces* **2014**, *6*, 5577; b) E. Sancaktar, in *Handbook of Adhesion Technology* (Eds: L. F. M. da Silva, A. Öchsner, R. D. Adams), Springer International Publishing, Cham, Switzerland **2018**, p. 283.
- [25] A. Zaban, L. Grinis, US/2012/0181573A1 **2012**.
- [26] A. Landau, US4409037A **1989**.
- [27] A. Zaban, L. Grinis, WO/2008/053464A2, **2009**.
- [28] G. Critchlow, in *Handbook of Adhesion Technology* (Eds: L. F. M. da Silva, A. Öchsner, R. D. Adams), Springer International Publishing, Cham, Switzerland **2018**, p. 131.
- [29] J. S. Liu, S. J. Lavery, P. Maguire, J. McLaughlin, J. Molloy, *J. Electrochem. Soc.* **1994**, *141*, L38.
- [30] a) F. Michalik, N. Luetzow, G. Schmidt, T. Huelsmann, M. Kloppisch, R. Haidar, P. Brooks, in *2015 10th Int. Microsystems, Packaging, Assembly and Circuits Technology Conf. (IMPACT)* (Eds.: M.-S. Yin, I. Lee), IEEE, Piscataway, NJ **2015**, pp. 83–87; b) B. J. Baliga, S. K. Ghandhi, *J. Electrochem. Soc.* **1977**, *124*, 1059.
- [31] J. J. Ponjee, H. J. Feil, US4093504A, **1978**.
- [32] D. McLean, B. Feldman, WO/1999/040235A1 **1999**.
- [33] I. Ahmet, R. v. d. Krol, F. F. Abdi, Y. Ma, WO/2019/052598, **2021**.
- [34] a) X.-L. Wang, M. Feyngenson, H. Chen, C.-H. Lin, W. Ku, J. Bai, M. C. Aronson, T. A. Tyson, W.-Q. Han, *J. Am. Chem. Soc.* **2011**, *133*, 11213; b) F. Xin, H. Zhou, Q. Yin, Y. Shi, F. Omenya, G. Zhou, M. S. Whittingham, *ACS Omega* **2019**, *4*, 4888.
- [35] R. M. Christensen, *Proc. R. Soc. A* **2020**, *476*, 20190719.
- [36] D. Briggs, *Surf. Interface Anal.* **1981**, *3*, 5.
- [37] M. C. Biesinger, B. P. Payne, A. P. Grosvenor, L. W. M. Lau, A. R. Gerson, R. S. C. Smart, *Appl. Surf. Sci.* **2011**, *257*, 2717.
- [38] M. C. Biesinger, L. W. M. Lau, A. R. Gerson, R. S. C. Smart, *Appl. Surf. Sci.* **2010**, *257*, 887.
- [39] a) W. Stumm, J. J. Morgan, *Aquatic Chemistry: Chemical Equilibria and Rates in Natural Waters*, Vol. 126, John Wiley & Sons, New York **2012**; b) B. Morgan, O. Lahav, *Chemosphere* **2007**, *68*, 2080.
- [40] a) M. H. Ahn, E. S. Cho, S. J. Kwon, *Vacuum* **2014**, *101*, 221; b) Y. Yang, Q. Huang, A. W. Metz, J. Ni, S. Jin, T. J. Marks, M. E. Madsen, A. DiVenere, S.-T. Ho, *Adv. Mater.* **2004**, *16*, 321.